Rensselaer

Department of Nuclear Engineering & Engineering Physics

March 31, 1993

Dr. Edwin P. Rood
Scientific Officer Code: 1132F
Office of Naval Research
800 North Quincy Street
Arlington, VA 22217-5000

Dear Dr. Rood:

The purpose of this letter is to transmit the ninth quarterly report for ONR Grant N00014-91-J-1271, "An Experimental Study of a Plunging Liquid Jet Induced Air Carryunder and Dispersion" (Lahey & Drew - Co-PI).

During this report period a technical paper entitled, "A Numerical Simulation of Two-Phase Jet Spreading Using an Eulerian-Lagrangian Technique," was accepted for presentation and publication at the 1993 Winter Annual Meeting of the ASME. A draft of this paper was previously transmitted to you by the eighth quarterly report and it has only needed to be slightly modified to resolve reviewer comments.

This report period was primarily concerned with performing mechanistic CFD predictions of a spreading two-phase jet using a multidimensional two-fluid model, and the comparison of these predictions with the data we have previously acquired. The attached paper, entitled, "A Numerical Simulation of a Turbulent Two-Phase Jet Using a Multidimensional Two-Fluid Model" has been prepared for submission to the *Int. J. Numerical Methods in Fluids.* As you can see the two-fluid model predictions agree fairly well with the data, however some trends have not yet been fully predicted. Moreover, more work is still required to properly model the air capture and spreading phenomenon as the liquid jet enters the pool. Nevertheless, these results are quite exciting since they show that mechanistic predictions of two-phase flow phenomena in free jets are indeed possible.

Finally, as I have previously reported to you, in early March I met with Professors Lasheras (UC-SD) and Loth (U. Illinois) in Pasadena to discuss research collaboration. In addition, I visited Professor Lasheras' laboratory in San Diego. It appears that research collaboration would be mutually beneficial and Professor

Drew and I plan to formally establish synergistic research collaboration in a future extension of this research project.

If you need any further information concerning this report please don't hesitate to contact me [(518) 276-8579] or Professor Drew [(518) 276-6903].

Sincerely yours,

Dr. R.T. Lahey, Jr.
The Edward E. Hood, Jr. Professor of Engineering

RTL/ev
Enclosure

cc: Administrative Grants Officer
       Director, Naval Research Laboratory
       Defense Technical Information Center
       D.A. Drew
       F. Bonetto

DTIC QUALITY

DRAFT

A NUMERICAL SIMULATION OF A TURBULENT TWO-PHASE JET USING A MULTIDIMENSIONAL TWO-FLUID MODEL

F. Bonetto, D.A. Drew, R.T. Lahey, Jr.
Center for Multiphase Research
Rensselaer Polytechnic Institute
Troy, NY 12180-3590 USA

CMR

INTRODUCTION

A good understanding of the air carryunder and bubble dispersion process associated with a plunging liquid jet is vital if one is to be able to quantify such diverse phenomena as sea surface chemistry, the meteorological significance of breaking ocean waves (eg, mitigation of the "greenhouse" effect due to the absorption of CO_2 by the oceans), the performance of certain type of chemical reactors, and a number of other important maritime-related applications.

The absorption of greenhouse gases into the ocean has been hypothesized to be highly dependent upon the air carryunder that occurs due to breaking waves. This process can be approximated with a plunging liquid jet [Monahan, 1991; Kerman, 1984]. Moreover, the air entrainment process due to the breaking bow waves of surface ships may cause long (ie, up to 5 km in length) wakes. Naturally, easily detectable wakes are undesirable for naval warships. In addition, the air carryunder that occurs at most hydraulic structures in rivers is primarily responsible for the large air/water mass transfer that is associated with these structures [Avery and Novak, 1978]. Also, air entrainment plays an important role in the slug flow regime. In particular, the liquid film surrounding a Taylor bubble has a flow in the opposite direction from the Taylor bubble. This liquid film can be thought of as a plunging liquid jet that produces a surface depression in the rear part of the Taylor bubble. When the annular liquid

93 4 09 062

93-07532

jet exceeds a critical velocity, it entrains small bubbles from the air in the Taylor bubble. These entrained bubbles follow the Taylor bubbles in the liquid slug.

Single-phase turbulent jets represent an important class of free shear flows that have been studied in the past to develop and test turbulence models [Abramovich, 1963]. More recently, turbulent jets have been evaluated numerically using computational fluid dynamic (CFD) techniques for various turbulence models. Rodi [1984] presented results using the classical k-ε model of Gibson & Launder [1976], and showed that k-ε models may not accurately predict jet spreading. Rodi [1984] proposed that the constant C_μ in the model for turbulent viscosity was really a function of the ratio between turbulent production and dissipation. This involved the development of a new function which produced better results. Sini and Dekeyser [1987] solved the single-phase turbulent jet using Rodi's k-ε model [Rodi, 1984]. This model compared favorably with the experimental results of the single-phase turbulent jet as well as with other more detailed algebraic stress models. Hence it appears that in some cases turbulent nonisotropy is not important and need not be modeled.

Significantly, it has been found that single-phase turbulent jet data can be used for the assessment of turbulence models because one does not have to constitute complicated turbulent closure laws near solid (no slip) boundaries. Indeed, due to the absence of walls and the associated shear boundary conditions the turbulent jet is probably the simplest non-trivial case to analyze. Interestingly, the same conclusions can be reached for a two-phase turbulent jet.

In most of the previously mentioned research, the flow field was considered to be thin in the lateral direction and the flows are characterized by a relatively small lateral velocity when compared to the streamwise velocity. This is equivalent to considering the flow (ie, the liquid jet) to be a boundary layer. Hence,

the flow is often assumed to have a negligible pressure gradient in the lateral direction, and the pressure in the boundary layer can be imposed by the external flow. From the mathematical point of view, this approximation changes the problem from an elliptic to parabolic one in the streamwise direction. From the computational point of view, when using a boundary layer approximation the pressure distribution has to be prescribed. That is, the static pressure as a function of the streamwise coordinate has to be known and supplied to the computational fluid dynamic (CFD) code.

Depending on the variables of interest, approximating the jet as a boundary layer may be a reasonable approximation. However, the lateral velocity at the edge of the jet (i.e., the entrainment velocity) may be much larger than the streamwise velocity. Moreover, for a planar jet the entrainment velocity remains finite as the integration domain in the lateral direction is enlarged.

In this work we did not make the boundary layer approximation. Rather, we assumed an elliptic problem for both the gas and the liquid phases. Solving the partial differential equations as an elliptic system increases the complexity of the problem but provides more detailed and accurate information on the flow field than a parabolic scheme. One of the advantages of the elliptic solution is that the streamwise pressure distribution does not have to be provided. This has two effects, first we are able to compute recirculation, and second, we are able to calculate the buoyancy-induced reversal of the bubbles. These two important effects cannot be computed using a parabolic approach.

In parabolic single-phase jet calculations using a k-ε model, Sini & Dekeyser [1987], and Hossain & Rodi [1982] found satisfactory agreement between calculations and experiments, except for a small region near jet inlet. Their good results are due in part to the fact that they analyzed a free jet which was only

weakly nonisotropic. The next level of complexity for simulating turbulent two-phase flows is the use of an Algebraic Stress Model (ASM). Several different models have been proposed in the literature. For the particular case of a planar jet, performance of the ASM is similar to the k-ε model. One might expect that the nonisotropic ASM model would produce better results than the isotropic k-ε model for the pressure distribution. However, when the ASM proposed by Gibson & Launder [1976] was used for the evaluation of a planar jet the computed streamwise-pressure distribution [Bergstrom, 1992] was virtually the same as when a k-ε model was used.

Thus, for simplicity, we have used a k-ε model in the computations presented in this paper. We note that the turbulence present in the liquid has two components in a two-phase jet. One component, the shear-induced turbulence, is due to viscosity and it is present in both single and two-phase flows. The other component is the bubble-induced turbulence due to slip between the bubbles and the surrounding liquid, and it only occurs in two-phase flows.

THE TWO-FLUID MODEL

Different phenomenologically-based models for two-phase flows have been proposed in the past. The drawback of many of these models is that they are only applicable to particular problems. On the other hand, mechanistically-based models, commonly known as Two-Fluid Models (TFM), have been proposed [Ishii, 1975; Delhaye, 1968 and Drew & Lahey, 1979].

For an adiabatic plunging liquid jet entraining air bubbles, we have the following local, instantaneous conservation equations:

Mass

$$\frac{\partial \rho_k}{\partial t} + \nabla \cdot (\rho_k \underline{v}_k) = 0 \qquad (k = g, \ell) \qquad (1)$$

Momentum

$$\frac{\partial}{\partial t}(\rho_k \underline{v}_k) + \nabla \cdot (\rho_k \underline{v}_k \underline{v}_k) = \nabla \cdot \underline{\underline{T}}_k + \rho_k \underline{g} \qquad (k = g, \ell) \qquad (2)$$

where,

$$\underline{\underline{T}}_k = -p_k \underline{\underline{I}} + \underline{\underline{\tau}}_k \qquad (3)$$

and, ρ_g, ρ_ℓ, $\underline{v}_g$, $\underline{v}_\ell$, p_g, p_ℓ, $\underline{\underline{\tau}}_g$, $\underline{\underline{\tau}}_\ell$ are the phasic densities, velocities, pressures and shear stresses of the gas and liquid phases, respectively.

These local, instantaneous conservation equations may be appropriately averaged to obtain the two-fluid model. Ishii [1975] and Delhaye [1968] have proposed time and spatial averages. However, the ensemble average [Drew & Lahey, 1979] seems to be the most fundamental type of averaging. An ensemble average is defined as,

$$\overline{f(\underline{x}, t)} = \int_S f(\underline{x}, t; \xi) P(\xi) d\xi \qquad (4)$$

were f is the function we want to average, $\underline{x}$ is the spatial coordinate, t is time, ξ is a parameter that determines a particular realization, $P(\xi)$ is the probability density function, and S is the set of all realizations. We note that $P(\xi)$ satisfies,

$$\int_S f(\underline{x}, t; \xi) d\xi = 1.0 \qquad (5)$$

Let us define the phase indicator function, $\chi_k(\underline{x}, t)$, such that it is unity if phase-k is present at $\underline{x}$ and time t, and is zero otherwise.

Thus, the volume fraction of phase-k, α_k, is,

$$\alpha_k = \overline{\chi_k} \tag{6}$$

The physical interpretation of α_k is as follows; $\alpha_k(\underline{x},t)$ is the fraction of all realizations in which phase-k is present at location $\underline{x}$ at time t.

We refer the reader to Arnold [1988] and Park [1992] for complete details on the derivation of the two-fluid model. We present here only the final results.

The ensemble-averaged continuity equation for phase-k is:

Mass

$$\frac{\partial\left(\alpha_k \overline{\rho}_k\right)}{\partial t} + \nabla \bullet \left(\alpha_k \overline{\rho}_k \overline{v}_k\right) = 0 \qquad\qquad (k = g \text{ or } \ell) \tag{7}$$

where,

$$\overline{\rho}_k = \frac{\overline{\chi_k \rho_k}}{\alpha_k} \tag{8}$$

is the ensemble-averaged phasic density.

In this work we assume that the gas and liquid densities are both constant, thus,

$$\overline{\rho}_k = \rho_k \frac{\overline{\chi}_k}{\alpha_k} = \rho_k \tag{9}$$

Next, $\overline{\underline{v}}_k$, the ensemble-averaged phasic velocity, is given by:

$$\overline{\underline{v}}_k = \frac{\overline{\chi_k \rho_k \underline{v}_k}}{\alpha_k \overline{\rho}_k} \cong \frac{\overline{\chi_k \underline{v}_k}}{\alpha_k} \tag{10}$$

The ensemble-averaged momentum equation for phase-k is:

Momentum

$$\frac{\left(\alpha_k \rho_k \bar{\underline{v}}_k\right)}{\partial t} + \nabla \cdot \left(\alpha_k \rho_k \bar{\underline{v}}_k \bar{\underline{v}}_k\right) = \nabla \cdot \left[\alpha_k \left(\bar{\bar{\underline{T}}}_k + \bar{\bar{\underline{T}}}_k^{Re}\right)\right]$$

$$+ \alpha_k \rho_k \underline{g} + \underline{M}_{ki} \qquad (k = g \text{ or } \ell) \qquad (11)$$

where, $\underline{T}_k, \underline{g}, \underline{M}_{ki}$ are the averaged stress tensor, the acceleration of gravity and the total interfacial forces, respectively. They are given by:

$$\bar{\bar{\underline{T}}}_k = \frac{\overline{\chi_k \underline{T}_k}}{\alpha_k} \qquad (12)$$

$$\bar{\bar{\underline{T}}}_k^{Re} = -\rho_k \overline{\underline{v}'_k \underline{v}'_k} \qquad (13)$$

where, $\underline{v}'_k$ is the fluctuation in the velocity of phase-k, and,

$$M_{ki} = -\overline{\underline{T}_k \cdot \nabla \chi_k} \qquad (14)$$

The ensemble averaged interfacial jump conditions are:

Interfacial Jump Conditions

$$\underline{M}_{gi} = -\underline{M}_{\ell i} + \nabla \cdot \left[\alpha_g \left(\underline{\underline{\sigma}}_s + \left(\overline{p_{gi}} - \overline{p_{\ell i}}\right)\right)\right] \qquad (15)$$

We note that, for monodispersed spherical bubbles, Laplace's equation yields,

$$\overline{p_{gi}} - \overline{p_{\ell i}} = 2\sigma / \bar{R}_b \qquad (16)$$

where, σ is the surface tension and $\bar{R}_b$ the mean bubble radius. The bubble's surface stress tensor, $\underline{\underline{\sigma}}_s$, is given by [Park, 1992],

$$\underline{\underline{\sigma}}_s \overset{\Delta}{=} \rho_\ell \left[\hat{a}_s \bar{\underline{v}}_r \bar{\underline{v}}_r + \hat{b}_s \left(\bar{\underline{v}}_r \cdot \bar{\underline{v}}_r\right)\underline{\underline{I}}\right] \qquad (17)$$

where, $\bar{v}_r \overset{\Delta}{=} \bar{v}_g - \bar{v}_\ell$, is the average relative velocity, and, using inviscid flow theory, the coefficients $\hat{a}_s$ and $\hat{b}_s$ in Eq. (17) can be analytically computed for spherical bubbles to be:

$$\hat{a}_s = -\frac{9}{20} \qquad , \qquad \hat{b}_s = \frac{3}{20} \tag{18}$$

TURBULENCE MODELING

The total Reynolds stress tensor for the continuous liquid phase is given by superposition as,

$$\underline{\underline{\tau}}_\ell^{Re} = \underline{\underline{\tau}}_{\ell(BI)}^{Re} + \underline{\underline{\tau}}_{\ell(SI)}^{Re} \tag{19}$$

where, for bubbly two-phase flows the bubble-induced shear stress is given by,

$$\alpha_\ell \underline{\underline{\tau}}_{\ell(BI)}^{Re} = -\frac{2}{3} \underline{\underline{A}}_{(BI)} \rho_\ell k_{\ell(BI)} \tag{20}$$

The bubble-induced turbulent kinetic energy, $k_{\ell(BI)}$, is given by Eq. (23a), where for potential flow around a sphere,

$$\underline{\underline{A}}_{(BI)} = \begin{pmatrix} 9/10 & 0 & 0 \\ 0 & 9/10 & 0 \\ 0 & 0 & 12/10 \end{pmatrix} \tag{21}$$

We note that $\underline{\underline{\tau}}_{\ell(SI)}^{Re}$ is the shear-induced Reynolds stress which comes from the classical k-ε model [Rodi, 1984]:

$$\frac{D_\ell[\alpha_\ell k_{\ell(SI)}]}{Dt} = \nabla \bullet \left[\alpha_\ell \upsilon_\ell^T \nabla k_{\ell(SI)} \right] + \alpha_\ell (P_\ell - \varepsilon_\ell) \tag{22a}$$

$$\frac{D_\ell[\alpha_\ell \varepsilon_\ell]}{Dt} = \nabla \bullet \left(\alpha_\ell \left[\frac{\upsilon_\ell^T}{Pr_\varepsilon^T} \right] \nabla \varepsilon_\ell \right) + \alpha_\ell (P_\varepsilon - \varepsilon_\varepsilon) \tag{22b}$$

where,

$$k_{\ell(BI)} = \frac{1}{2}\,\alpha_g\,C_{vm}\,|\bar{\underline{v}}_r|^2 \tag{23a}$$

$$k_\ell = k_{\ell(SI)} + k_{\ell(BI)} \tag{23b}$$

$$\upsilon_\ell^T = C_\mu\,C_d\,\frac{k_{\ell(SI)}^2}{\varepsilon_\ell} \tag{23c}$$

$$P_\ell = \upsilon_\ell^t\,(\nabla\bar{\underline{v}}_\ell + \bar{\underline{v}}_\ell\,\nabla):\nabla\underline{v}_\ell \tag{23d}$$

$$P_\varepsilon = C_{1e}\,\frac{\varepsilon_\ell P_\ell}{k_{\ell(SI)}} \tag{23e}$$

$$\varepsilon_\varepsilon = C_{2e}\,\varepsilon_\ell^2/k_{\ell(SI)} \tag{23f}$$

$$Pr_\varepsilon^T = 1.3 \tag{23g}$$

and [Rodi, 1984], $C_\mu = 0.5478$, $C_d = 0.1643$, $C_{1e} = 1.44$, $C_{2e} = 1.92$ are the single-phase flow k-ε model coefficients.

Using these results, the Reynolds stress tensor is given by:

$$\underline{\underline{\tau}}_{\ell(SI)}^{Re} = \upsilon_\ell^T\left[\nabla\bar{\underline{v}}_\ell + \bar{\underline{v}}_\ell\nabla\right] \tag{24}$$

After averaging, we have more unknowns than equations. Thus, we need to constitute some of the averaged quantities in terms of the state variables, α_k, $\bar{\underline{v}}_k$ and $\bar{p}_k$. This closure process is necessary because we have lost information due to averaging and we must reintroduce the essential physics which was lost.

Cell model averaging was successfully applied to a dilute mixture of liquid and gas bubbles by Arnold [1988] and Park [1992]. As can be seen in Figure-1, we divide the flow field into "cells", each of which have only one spherical bubble inside. Using inviscid flow theory we may compute the pressure distribution

around the bubbles and thus deduce the various interfacial forces. The assumptions are that both phases are inviscid, incompressible and have constant thermophysical properties, the bubbles are spherical and can be treated as a dilute dispersion of spheres, the non-uniformities in the distribution of the dispersed phase are small and the velocity gradients of both phases are small.

Figure-1 shows a typical cell for one particular realization of the ensemble. Note that $\underline{x}$ is the vectoral location under consideration, $\underline{z}$ is the position of the center of the bubble in a particular realization of the ensemble, and $\underline{x}' = \underline{x} - \underline{z}$ is the position of the bubble with respect to $\underline{x}$, the location under consideration. We need to constitute the following quantities: $\underline{\underline{T}}_k^{Re}$, $\underline{\underline{T}}_k$, $\underline{M}_{ki}$, $\bar{p}_{ki}$ in terms of the state variables.

Using the results of Arnold [1988] and Park [1992] the resultant two-fluid phasic momentum equations are:

Momentum Conservation - Gas Phase

$$\frac{\partial}{\partial t}(\alpha_g \rho_g \bar{\underline{v}}_g) + \nabla \bullet (\alpha_g \rho_g \bar{\underline{v}}_g \bar{\underline{v}}_g) = - \alpha_g \nabla \bar{p}_\ell$$

$$- C_{vm} \alpha_g \rho_\ell \left[\left(\frac{\partial}{\partial t} + \bar{\underline{v}}_g \bullet \nabla \right) \bar{\underline{v}}_g - \left(\frac{\partial}{\partial t} + \bar{\underline{v}}_\ell \bullet \nabla \right) \bar{\underline{v}}_\ell \right]$$

$$- C_{rot} \alpha_g \rho_\ell \bar{\underline{v}}_r \times \nabla \times \bar{\underline{v}}_g - C_L \rho_\ell \alpha_g \bar{\underline{v}}_r \times \nabla \times \bar{\underline{v}}_\ell$$

$$- (C_1 + C_2 - 2C_p - 2b_s) \alpha_g \rho_\ell \bar{\underline{v}}_r \bullet \nabla \bar{\underline{v}}_r^T + (a_s - C_2) \alpha_g \rho_\ell \bar{\underline{v}}_r \bullet \nabla \bar{\underline{v}}_r$$

$$+ (a_s - C_2) \alpha_g \rho_\ell (\nabla \bullet \bar{\underline{v}}_r) \bar{\underline{v}}_r + \alpha_g \rho_g \underline{g} - \frac{C_D}{8} \rho_\ell A_i''' \bar{\underline{v}}_r |\bar{\underline{v}}_r| - C_{TD} \rho_\ell k_\ell \nabla \alpha_g \qquad (25a)$$

Momentum Conservation - Liquid Phase

$$\frac{\partial}{\partial t}(\alpha_\ell \rho_\ell \bar{v}_\ell) + \nabla \bullet (\alpha_\ell \rho_\ell \bar{v}_\ell \bar{v}_\ell) = -\alpha_\ell \nabla \bar{p}_\ell + (C_p + b_s + b_\ell)\rho_\ell |\bar{v}_r|^2 \nabla \alpha_g$$

$$+ C_{vm}\alpha_g \rho_\ell \left[\left(\frac{\partial}{\partial t} + \bar{v}_g \bullet \nabla\right)\bar{v}_g - \left(\frac{\partial}{\partial t} + \bar{v}_\ell \bullet \nabla\right)\bar{v}_\ell\right]$$

$$+ C_{rot}\alpha_g \rho_\ell \bar{v}_r \times \nabla \times \bar{v}_g + C_L \rho_\ell \alpha_g \bar{v}_r \times \nabla \times \bar{v}_\ell + (C_2 + a_\ell)\alpha_g \rho_\ell \bar{v}_r (\nabla \bullet \bar{v}_r)$$

$$+ (C_1 + C_2 + 2b_\ell)\alpha_g \rho_\ell \bar{v}_r \bullet \nabla \bar{v}_r^T + (C_2 + a_\ell)\alpha_g \rho_\ell \bar{v}_r \bullet \nabla \bar{v}_r$$

$$+ (a_s + a_\ell)\rho_\ell (\bar{v}_r \bullet \nabla \alpha_g)\bar{v}_r + \alpha_\ell \rho_\ell g + \frac{C_D}{8}\rho_\ell A_i''' \bar{v}_r |\bar{v}_r| + C_{TD}\rho_\ell k_\ell \nabla \alpha_g \quad (25b)$$

where both phases were assumed to be incompressible.

For numerical purposes it is important to rewrite Eq. (25a) as follows. For the air/water flows under consideration Eq. (7) can be employed to show that the left hand side of the gas phase momentum equation can be rewritten in Lagrangian form as:

$$\frac{\partial}{\partial t}(\alpha_g \rho_g \bar{v}_g) + \nabla \bullet (\alpha_g \rho_g \bar{v}_g \bar{v}_g) = \rho_g \alpha_g \frac{D\bar{v}_g}{Dt} \quad (26)$$

Grouping the right hand side of Eq. (26) with one part of the virtual mass force in Eq. (25a) we obtain:

$$\rho_g \alpha_g \frac{D\bar{v}_g}{Dt} + C_{vm}\rho_\ell \alpha_g \frac{D\bar{v}_g}{Dt} = (\rho_g + C_{vm}\rho_\ell)\alpha_g \frac{D\bar{v}_g}{Dt} \quad (27)$$

Notice that we have kept the other part of the virtual mass force associated with liquid phase acceleration in the second term on the right hand side of Eq. (25a). It has been found that writing the gas phase's acceleration as in Eq. (27) promotes numerical convergence.

Equations (25) were numerically evaluated using the finite difference formulation of Patankar [1980] in the well-known PHOENICS code. First the domain of interest (DOI) was subdivided into a Cartesian grid, as shown in Fig. 2. The dependent variables were calculated and stored at discrete points on the grid. To prevent pressure "checker boarding" [Patankar, 1980] a staggered grid was used. The velocities are calculated at the locations, shown by the arrows in Fig. 2 that are between pressure points (P). The cell surrounding point P is often called the continuity cell. The velocities, $\bar{v}_y$ and $\bar{v}_z$, were computed at the arrow locations and the pressure and void fraction, $\bar{p}_\ell$ and α_g, were computed at the continuity cell center (P).

According to the differencing procedure, the conservation equations were first integrated over the control volume that surrounds the node. The resulting integrals were then approximated using the nodal values and algebraic difference equations were obtained, where the discrete equations had an implicit formulation.

Implementation of the various source terms required special attention. We have used lagged quantities for them, (i.e., values from the previous iteration). Even though there are many terms on the right hand side of the conservation equations, all of them can be written as a function of the following quantities: α_g, $\nabla\alpha_g$, $\bar{\underline{v}}_k$ and $\nabla\bar{\underline{v}}_k$. Notice that α_g is naturally given at the continuity cell center and $\nabla\alpha_g$ is computed using a first order Taylor series expansion at locations w, e, s and n (Fig. 2). The velocity component, $\bar{v}_{ky}$, was given at locations w,e and $\underline{v}_{kz}$ was given at locations n,s. Finally, $\nabla\bar{v}_k = \bar{v}_{kj,i}$ was computed using a first order Taylor series expansion and the locations are P, nw, ne, sw, se depending on the velocity components j and the coordinate i. Because these four basic quantities are naturally given at different locations, we need to perform some kind of averaging

before computing the source terms. To illustrate this let us take as an example the lift force in the y-direction. The lateral force is proportional to:

$$\text{Lift}_y \propto \alpha_g \, (\bar{v}_{gy} - \bar{v}_{\ell y}) \left(\frac{\partial \bar{v}_{\ell y}}{\partial z} - \frac{\partial \bar{v}_{\ell z}}{\partial y} \right) \tag{28}$$

were α_g is given at the continuity cell center, P (Fig. 3), $\nabla \alpha_g$ at w, e, s and n, $\bar{v}_{\ell y}$ is given a w,e, $\bar{v}_{\ell y,z}$ is given at nw and $\bar{v}_{\ell z,y}$ is given at ne. It is not consistent to multiply quantities given at different locations. After some experimentation we obtain acceptable convergence speed and accuracy with the following criteria. All tensor components with repeated indices (T_{11}, T_{22}, ...) were computed at the continuity cell center P. Off-diagonal tensor components (T_{12}, ...) were computed at corresponding continuity cell corners (eg, ne for the case of index 12).

In order to numerically evaluate the two-fluid model we also needed the appropriate boundary and initial conditions. There is no general theory for the type of boundary and initial conditions that a system of nonlinear partial differential equations requires in order to have a unique solution. Many researchers in the past have evaluated two-phase models as initial value problems using parabolic numerical techniques, thus it was not necessary to specify boundary conditions at the outlet of the integration domain. However, as discussed previously, when this approach is used, one has to specify the pressure distribution in the integration domain. For many cases a hydrostatic pressure distribution was a good enough approximation. However, when a parabolic scheme is used, one cannot compute flow recirculation nor buoyancy-induced gas reversal, an important feature of the two-phase jets which are of interest in this study.

As noted previously, in this work we used an elliptic (ie, boundary value) calculational scheme. That is, we numerically evaluated the full two-fluid model

and the associated k-ε model using appropriate boundary conditions at the inlet and the exit of the flow domain. This complicated the evaluation procedure, however only in this way could we obtain an accurate prediction for the gas phase.

Figure-3 shows the integration domain. Note that we have refined the grid near the symmetry plane of the planar jet because the gradients are the steepest there. In the axial (i.e., z) direction we have increasingly larger cells because of the decreasing gradients. The boundary conditions which have been used are:

<u>INLET</u> $(z = 0, -\frac{h}{2} \leq y \leq \frac{h}{2})$

$$\text{Gas mass flux} = \alpha \, \rho_g \, V \tag{29a}$$

$$\text{Liquid mass flux} = (1 - \alpha) \, \rho_\ell \, V \tag{29b}$$

$$\bar{u}_{\ell y} = 0 \tag{29c}$$

$$\bar{u}_{gy} = 0 \tag{29d}$$

$$\bar{u}_{\ell z} = V \tag{29e}$$

$$\bar{u}_{gz} = V \tag{29f}$$

$$\text{Kinetic energy} \equiv k_\ell = \frac{3}{2} \left(\bar{u}'_{\ell z}\right)^2 \tag{29g}$$

$$\text{Dissipation} \equiv \varepsilon = \frac{\left(\bar{u}'_{\ell z}\right)^3}{C_\mu^{1/4} \, h} = 1.8256 \left(\bar{u}'_{\ell z}\right)^3 / h \tag{29h}$$

<u>OUTLET</u> $(z = Z)$

$$p = \rho_\ell g \, Z \cos \theta \tag{30a}$$

$$\frac{\partial \bar{u}_{\ell y}}{\partial z} = 0 \qquad\qquad \frac{\partial \bar{u}_{gy}}{\partial z} = 0 \tag{30b}$$

$$\frac{\partial \bar{u}_{\ell z}}{\partial z} = 0 \qquad\qquad \frac{\partial \bar{u}_{gz}}{\partial z} = 0 \tag{30c}$$

$$\frac{\partial k}{\partial z} = 0 \qquad\qquad \frac{\partial \varepsilon}{\partial z} = 0 \qquad\qquad (30d)$$

It should be noted that the boundary conditions associated with the mass balances are only required at the inlet. This can be understood based on the fact that the mass balance is a first order partial differential equation. Moreover, given the velocity field, the equation may be solved for the void fraction along the model's characteristics. With the void fraction given at the inlet, the void fraction field can be readily evaluated.

Because the velocity fields, as well as the turbulent kinetic energy and the dissipation, are not well known at the outlet, we specified natural boundary conditions there. That is, we set the gradients of these variables in the flow direction equal to zero. Fortunately, in our case, the outlet boundary conditions were found to have a negligible effect, except for the last two rows of cells.

The numerical results presented herein correspond to a planar liquid jet impacting a liquid pool using the two-fluid model previously discussed. The liquid jet velocity at the location of impact was $\bar{u}_{\ell z} = 5$ m/s, and a constant bubble diameter of 2mm was assumed. The initial velocity profile was uniform. The jet width, h, was 4.03 mm, and the void fraction at the location of impact was assumed to be uniform and equal to 5%. The inlet turbulent intensity was 3% and the inlet dissipation was computed. The inclination angle of the jet was measured with respect to the vertical plane (i.e. $\theta = 0°$ means a vertical planar jet). The integration domain had an extent of y = 0.2 m in the lateral direction and z = 0.25 m in the axial direction. The k-ε model for turbulence employed the constant values suggested by Rodi [1984] for single-phase flow.

We have presented results corresponding to a vertical liquid jet ($\theta = 0°$, z = 0.225 m; note, y = 0.1 m is the jet's plane of symmetry). Both velocity profiles show

a Gaussian-like profile. We see that, due to buoyancy, the liquid velocity is always higher than the gas velocity, a well-known characteristic of bubbly two-phase downflows. Moreover, the relative velocity was approximately 0.3 m/s which is very close to the terminal rise velolcity of the single bubbles.

Figure-5 shows the axial liquid velocity as a function of lateral position for different axial positions. The curve labeled, $z = 0.00125$ m, is right under the location of jet impact and one can see an almost uniform velocity profile ($\bar{u}_z \cong$ 5 m/s). As we move down in the pool the jet is dispersed due to momentum interchange with the surrounding fluid. The curve $z = 0.225$ m is the same one shown in Figure 4 for liquid velocity.

Figure-6 shows the turbulent kinetic energy, k_ℓ, as a function of lateral position for $z = 0.225$ m. The curve shows the characteristic relative minimum in k_ℓ at the symmetry plane.

In Figure-7 the liquid velocity field has been plotted as a function of axial and lateral position. The length of the arrows is proportional to the liquid velocity at the location of the arrow's tail. The arrow's tail is located at the center of the computational cell. The arrow scale is in the lower left corner ($u_{z\ell} = 2$ m/s). The spreading of the jet can be easily seen in this plot, as noted previously. Near the location of jet impact ($z = 0$) the axial velocity is almost uniform. Because of the momentum interchange between the jet and the surrounding fluid, liquid is entrained in the lateral, y, direction. Finally, one may note the formation of two weak recirculation zones near the y-boundaries for large z.

Figure-8 shows a contour plot of the axial liquid velocity. The lines connect positions with the same axial velocity (equivelocity lines). The outer curve corresponds to $\bar{u}_{z\ell} = 0.25$ m/s, and the difference between successive lines is 0.25 m/s.

Figure-9 shows a contour plot of the void fraction for one half of the jet. The outer line connects points with the void fraction $\alpha = 0.25\%$.

Figure-10 shows a vector plot of the liquid velocity field for an inclined planar jet ($\theta = 45°$). We have rotated the integration domain 45° in order to have the plane $y = 0$ aligned with the jet orientation. This was done to minimize numerical diffusion. It can be seen that, as expected, the rising gas drags the liquid away from the centerplane.

Figure-11 shows a vector plot of the gas velocity field for an inclined planar jet ($\theta = 45°$). Of particular interest are the results shown in the upper right corner, the gas velocity (weighted by the local void fraction) at the y-boundary which shows flow reversal of the gas.

COMPARISON WITH EXPERIMENTS

The results presented in the previous section have inlet boundary conditions that are the simplest to implement for the two-phase jet. The average axial liquid velocity, $\bar{v}_{\ell z}$, and the liquid turbulent kinetic energy, k_ℓ, were assumed to be uniform in the liquid jet cross section. These are good approximations for the experiments we have compared the calculation against [Bonetto & Lahey, 1993]. However, the assumption of a uniform inlet void fraction distribution was too crude. We re-evaluated the two-fluid model, but instead of using the boundary conditions given in Eq. (29), we used the average axial liquid and gas velocities, $\bar{v}_{\ell z}$ and $\bar{v}_{g z}$, the liquid turbulent kinetic energy, $\overline{v'^2_{\ell z}}$, and the gas void faction α_g that were actually measured at the inlet of the integration domain. Figure 12 shows the average axial liquid velocity, $\bar{v}_{\ell z}$. The open circles are the experimental values at the inlet of the domain. The solid curve is the

computed $\bar{v}_{\ell z}$ at the axial position z = 2.5 mm (i.e., at the first velocity node), and y = 0.1 m corresponds to the planar jet's centerplane.

Figure 13 shows the computed $\bar{v}_{\ell z}$ at z = 31 mm. The open circles are experimental points. We can see that the agreement is quite good. The spreading of the jet is well predicted and the underprediction at the center line velocity is similar to that observed in single-phase flows [Rodi, 1984]. Figure-14 shows the computed $\bar{v}_{\ell z}$ at z = 59 mm. The open circles are again experimental points, and the trend is similar to Fig. 13.

Figure-15 shows the gas volume fraction as a function of the lateral position. The open circles are the experimental values. The solid curve is the computed α_g at the axial position z = 1.25 mm (i.e. at the first gas volume faction node). Figure 16 and 17 show the gas volume fraction as a function of the lateral position at distances from the integration domain inlet of z = 31 mm and z = 89 mm, respectively. We can see that the agreement is good. However it can be noticed that the model tends to overpredict gas dispersion. In Fig. 17 the experimental peaks are higher than the predicted ones and the experimental center plane valley is somewhat deeper than predicted.

SUMMARY AND CONCLUSIONS

A state-of-the-art two-fluid model obtained using ensemble averaging has been derived and was closed using cell average model. This approach provides equations for multiphase flows that are mechanistically-based (as opposite to empirical). The rigorous derivation of the cell average model provides exact constitutive equations for the inviscid limit. One does not expect the values of the constants from cell model averaging to be correct for very viscous flows but they provide a good framework to start from. In particular, it is known [Wang et al,

1987] that the lift coefficient, C_L, decreases as liquid viscosity increases. In this study, a lift force coefficient of C_L = .05 has been used instead of the inviscid limit value of C_L = .25. All other parameter values used in this work corresponded to the inviscid limit values. The agreement with the experiments is remarkable.

The k-ε model seems to be adequate for this calculation, however the observed differences in phasic dispersion indicate some inadequacies in the turbulence modeling which should be considered in future studies.

ACKNOWLEDGMENTS

REFERENCES

Abramovich, G.N., "The Theory of Turbulent Jets," MIT Press, 1963.

Arnold, G., "Entropy and Objectivity as Constraints Upon Constitutive Equations for Two-Phase Modeling of Two-Phase Flows," Ph.D. Thesis, Rensselaer Polytechnic Institute, 1988.

Avery, S. & Novak, P., "Oxygen Transfer at Hydraulic Structures," *Journal of Hyd. Div.*, ASCE, Vol. 104(HY11), pp. 1521-1540, 1978.

Bergstrom, D.J., "A Prediction of the Pressure Field in a Plane Turbulent Jet Using an Algebraic Stress Model," *Int. J. Numerical Methods in Fluids*, Vol. 14, pp. 907-918, 1992.

Bonetto, F. and Lahey, R.T., Jr., "Experimental Results of a Two-Phase Planar Jet," in preparation, 1993.

Chen, C.J. and Rodi, W., "Turbulent Buoyant Jets - A Review of Experimental Data," HMT, Vol. 4, Pergamon, Oxford, 1980.

Delhaye, J.M., "Equations Fondamentales des Ecoulement Diphasiques, Part I and II," CEA-R-3429, Centre d'Etudes Nucleaires de Grenoble, France, 1968.

Drew, D.A. and Lahey, R.T., Jr., "Application of General Constitutive Principles to the Derivation of Multidimensional Two-Phase Flow Equations," *Int. J. Multiphase Flow*, Vol. 5, pp. 423-264, 1979.

Gibson, M.M. and Launder, B.E., "On the Calculation of Horizontal, Turbulent, Free Shear Flows Under Gravitational Influence," *J. Heat Transfer*, ASME, Vol. 98, p. 81-87, 1976.

Hossain, M.S. and Rodi, W., "A Turbulence Model for Buoyant Flows and Its Application to Vertical Buoyant Jets," in W. Rodi (ed.), "Turbulent Jets and Plumes," HMT, Vol. 6, Pergamon, New York, 1982, pp. 121-178.

Ishii, M., "Thermo-Fluid Dynamic Theory of Two-Phase Flow," Eyrolles, 1975.

Kerman, B.R., "A Model of Inerfacial Gas Transfer for a Well-Roughened Sea," *Journal of Geophysical Research*, Vol. 89(D1), pp. 1439-146, 1984.

Launder, B.E. and Spalding, D.B., "Lectures in Mathematical Models of Turbulence," Academic Press, New York, 1972.

Monahan, L. and Torgersen, T., in *Air Water Mass Transfer*, edited by S. Wilhelms and J. Gulliver, American Society of Civil Engineers, 1991.

Park, J.W., "Void Wave Propagation in Two-Phase Flow," Ph.D. Thesis, Rensselaer Polytechnic Institute, 1992.

Patankar, S.V., "Numerical Heat Transfer and Fluid Flows," Hemisphere Publishing Corp., 1980.

Raithby, G.D., Galpin, P.F., Van Doormal, J.P., "Prediction of Heat and Fluid Flow in Complex Geometries Using General Orthogonal Coordinates," *Numer. Heat Transfer*, Vol. 9, pp. 125-142, 1986.

Rodi, W., "Turbulence Models and their Application in Hydraulics," IAHR/AIRH Monograph, 1984.

Sini, J.F., and DeKeyser, I., "Numerical Prediction of Turbulent Plane Jets and Forced Plumes by Use of the k-ε Model of Turbulence," *Int. J. Heat Mass Transfer*, Vol. 30, No. 9, pp. 1787-1801, 1987.

Wang, S.K., Lee, S-J., Lahey, R.T., Jr. and Jones, O.C., Jr., "3-D Turbulence Structure and Phase Distribution Measurements in Bubbly Two-Phase Flows," *Int. J. Multiphase Flow*, Vol. 13, No. 3, pp. 327-343, 1987.

Figure 1   Unit Cell
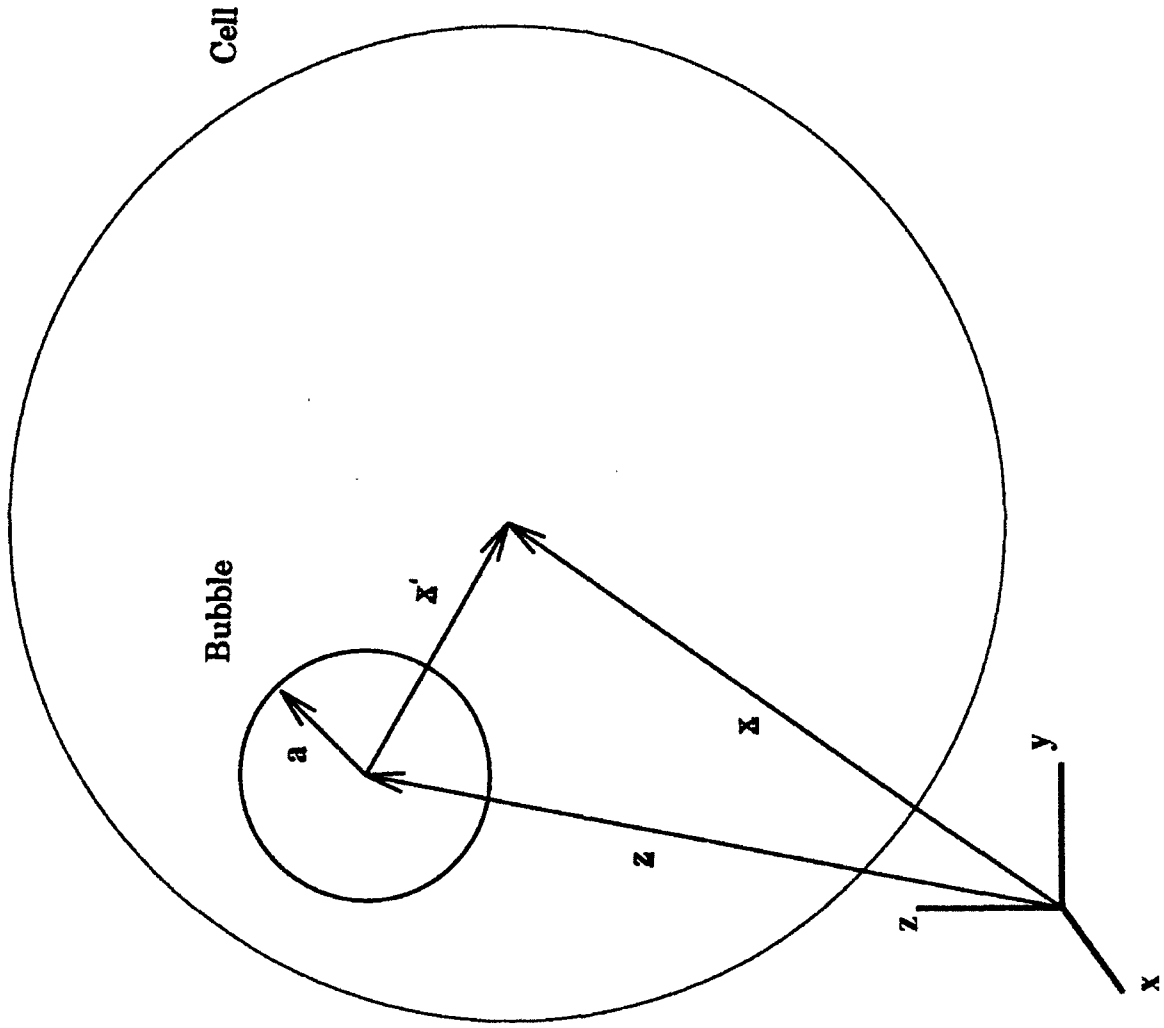
Figure 2   Control Volumes
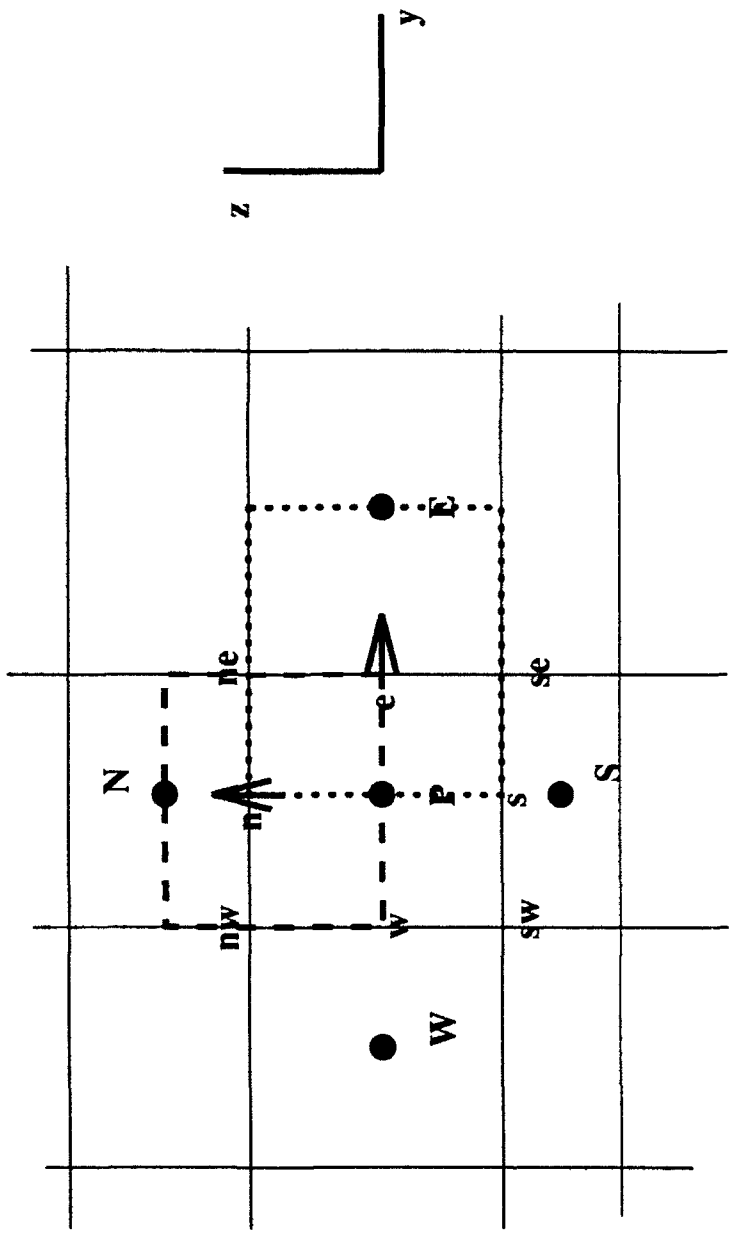
········· velocity cell in y direction

— — · velocity cell in z direction

Figure 3   Discretization of the Integration Domain

K-EP, PLANAR JET, ELLIPTIC, FABIAN, 2 PHASE,

PHOENICS
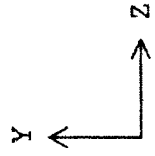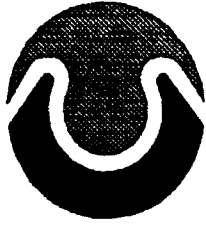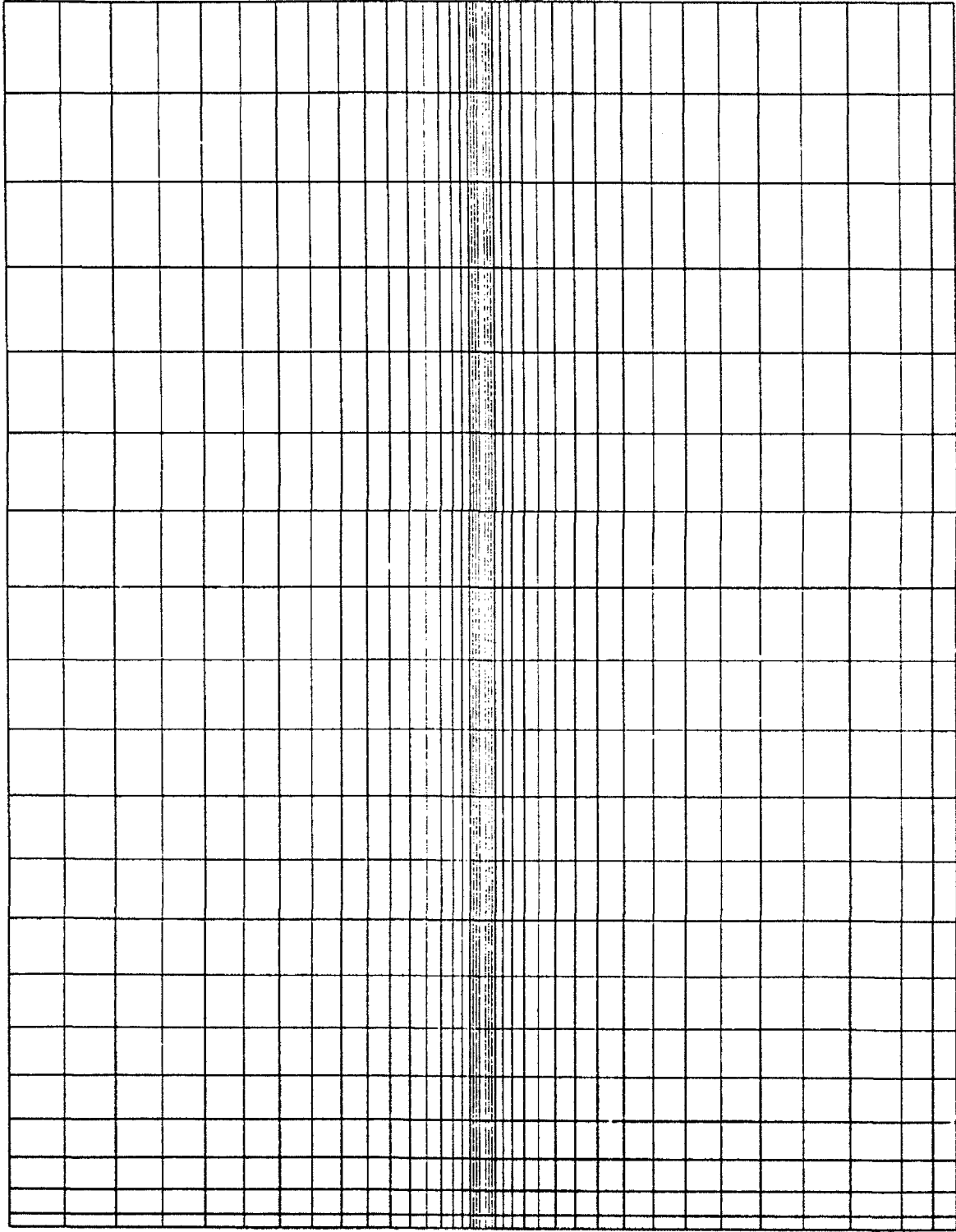
Figure 4   Liquid and Gas Velocity Profiles for an Axial Position
            z = 0.225 m
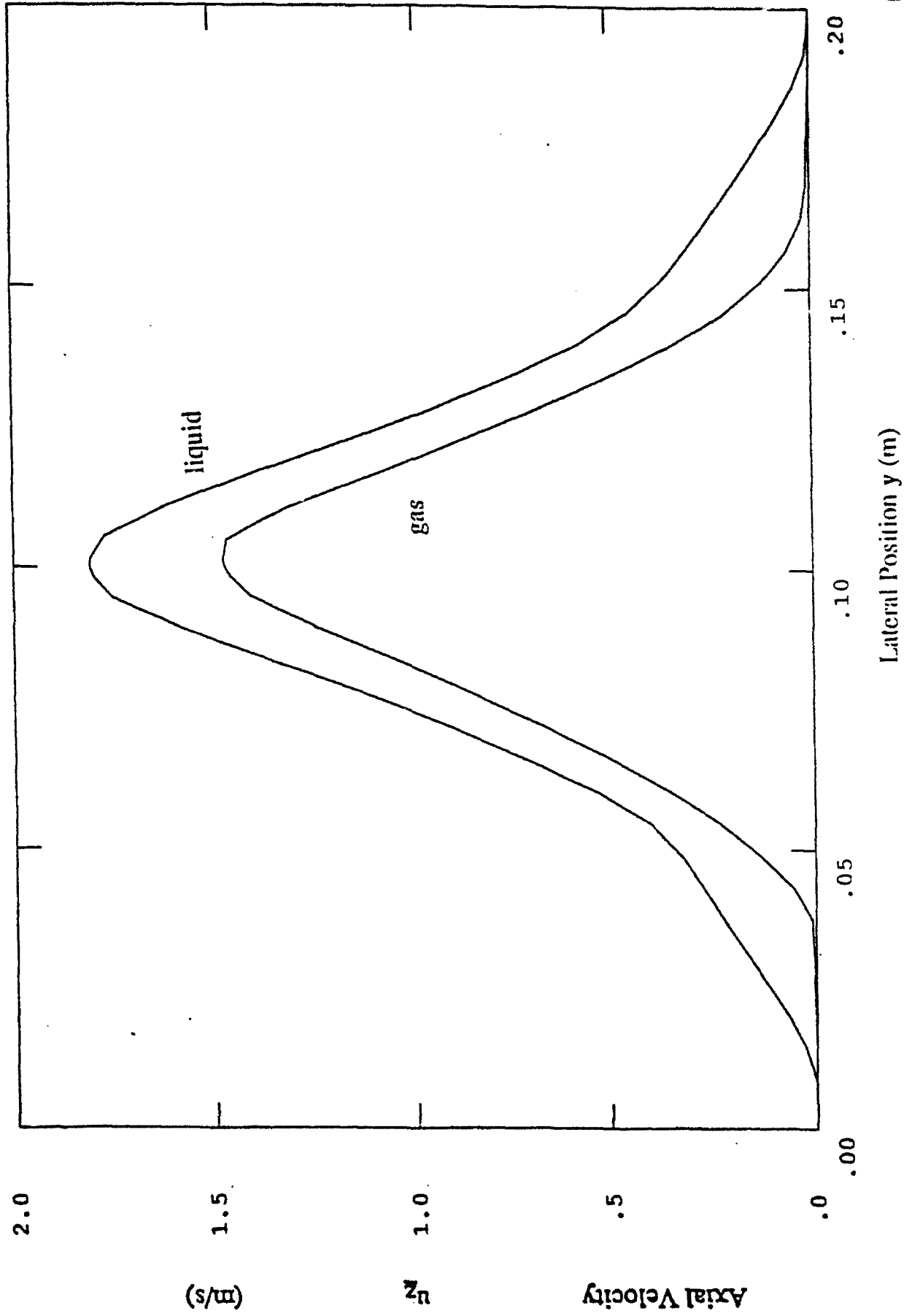
**Figure 5   Liquid Velocity Profiles for Four Different Axial Positions**

z = 0.00125 m

z = 0.0325 m

z = 0.085 m

z = 0.225 m

Lateral Position y (m)

Axial Velocity u_z (m/s)
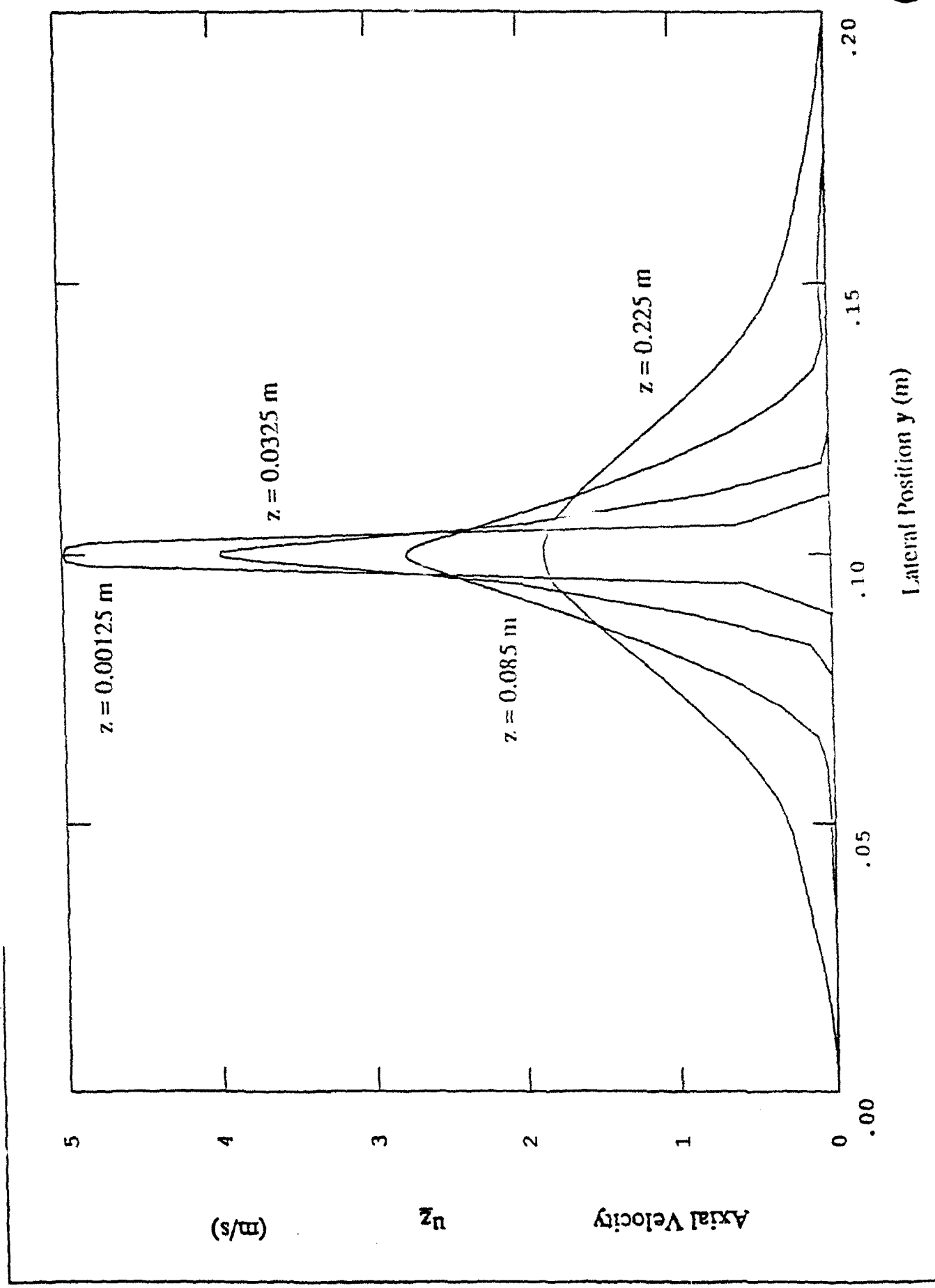
Figure 6   Turbulent Kinetic Energy Profiles for z = 0.225 m

z = 0.225 m

Lateral Position y (m)
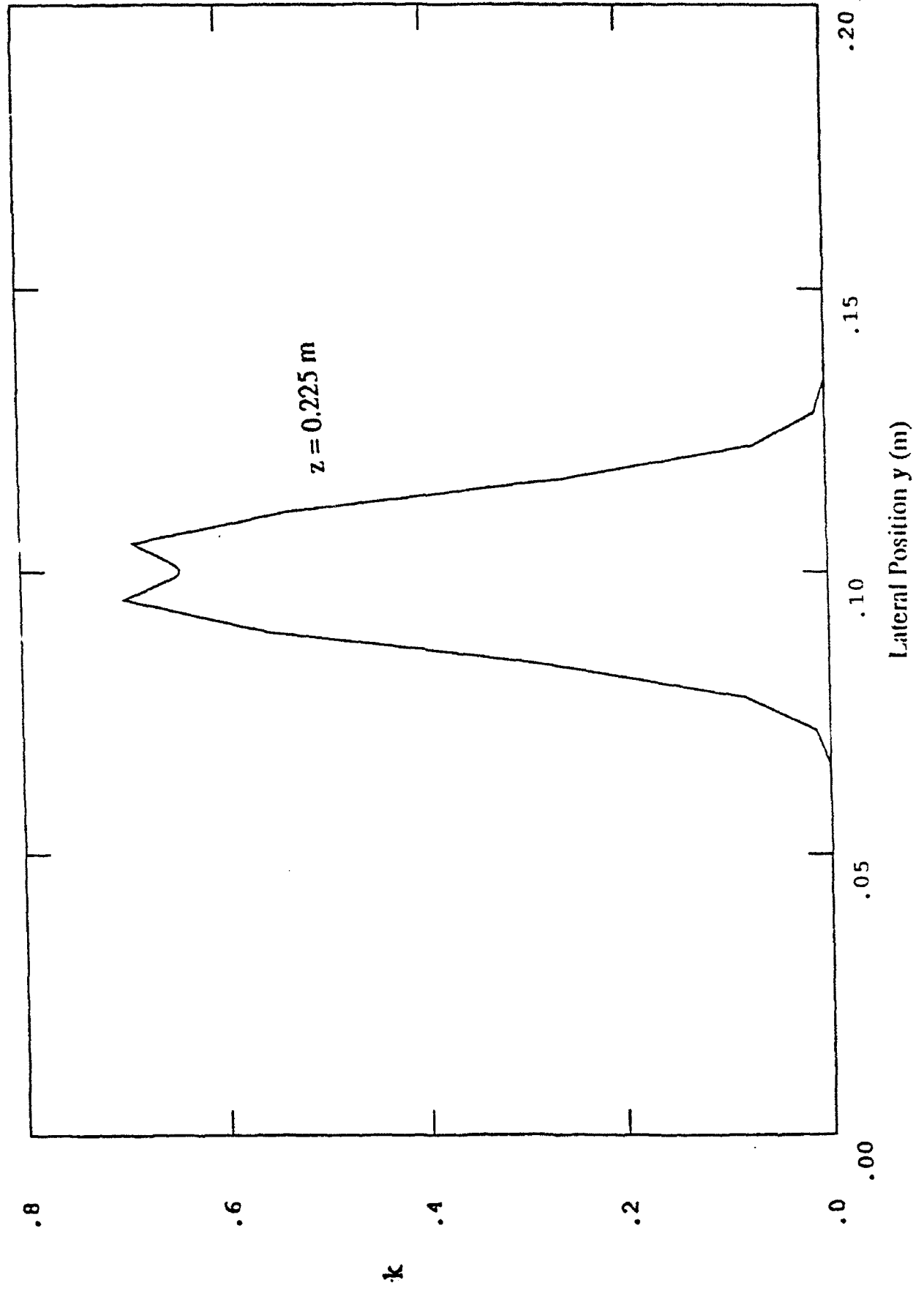
Figure 7   Vector Plot of the Liquid Velocity for θ = 0°

θ = 0 degrees

liquid

→ : 2.00 m/s.

K-EP, PLANAR JET, ELLIPTIC, FABIAN, 1 PHASE,

PHOENICS

Figure 8   Contour Plot of the Axial Liquid Velocity for $\theta = 0^\circ$

$\theta = 0$ degrees

liquid

Y ← Z

K-EP, PLANAR JET, ELLIPTIC, FABIAN, 1 PHASE,
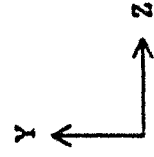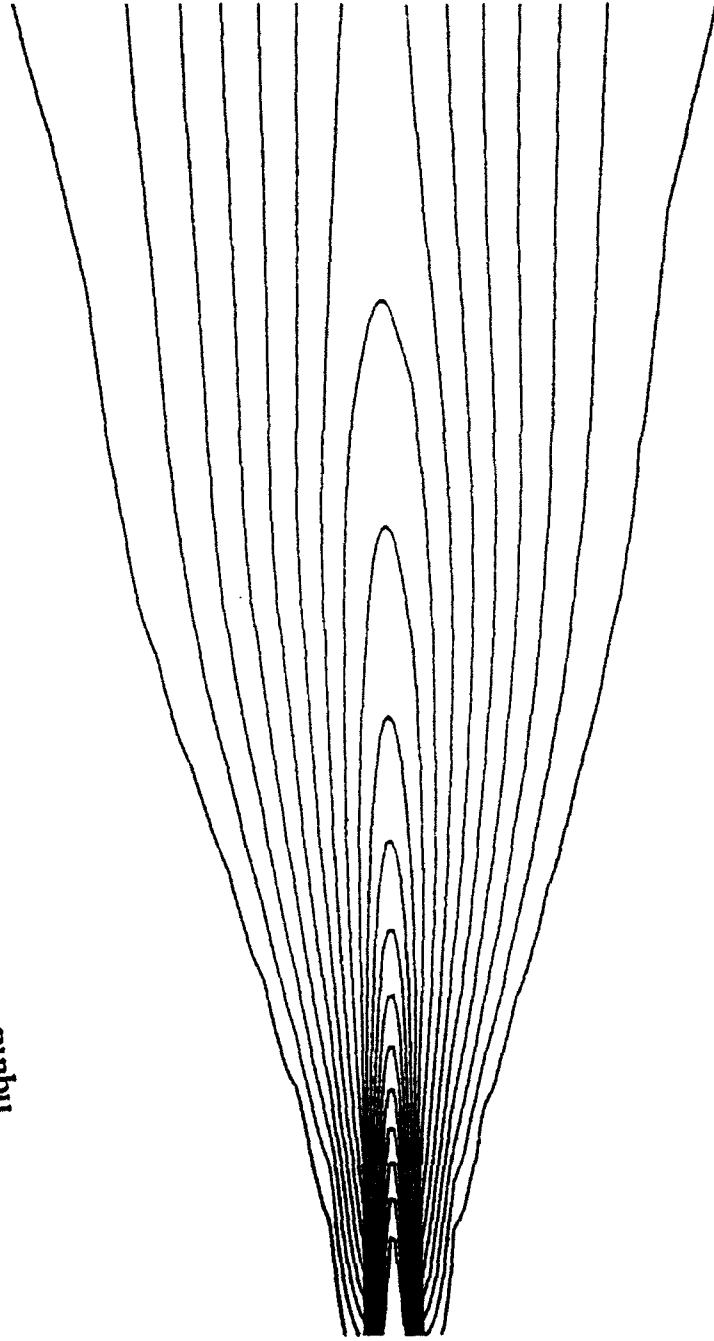
Figure 9 Contour Plot of the Void Fraction (Half of the Jet) for the Vertical Jet
(θ = 0°)

θ = 0 degrees

(gas)
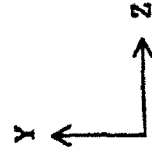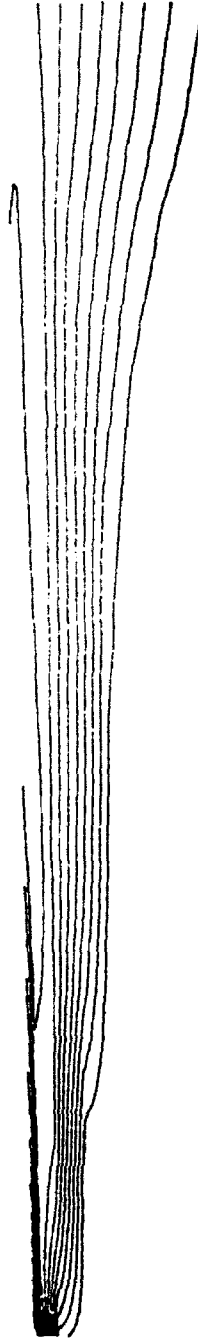
Figure 10 Vector Plot of the Liquid Velocity of the Inclined Jet ($\theta = 45°$)

$\theta = 45$ degrees

liquid

$\bar{u}_\ell$ (45°)
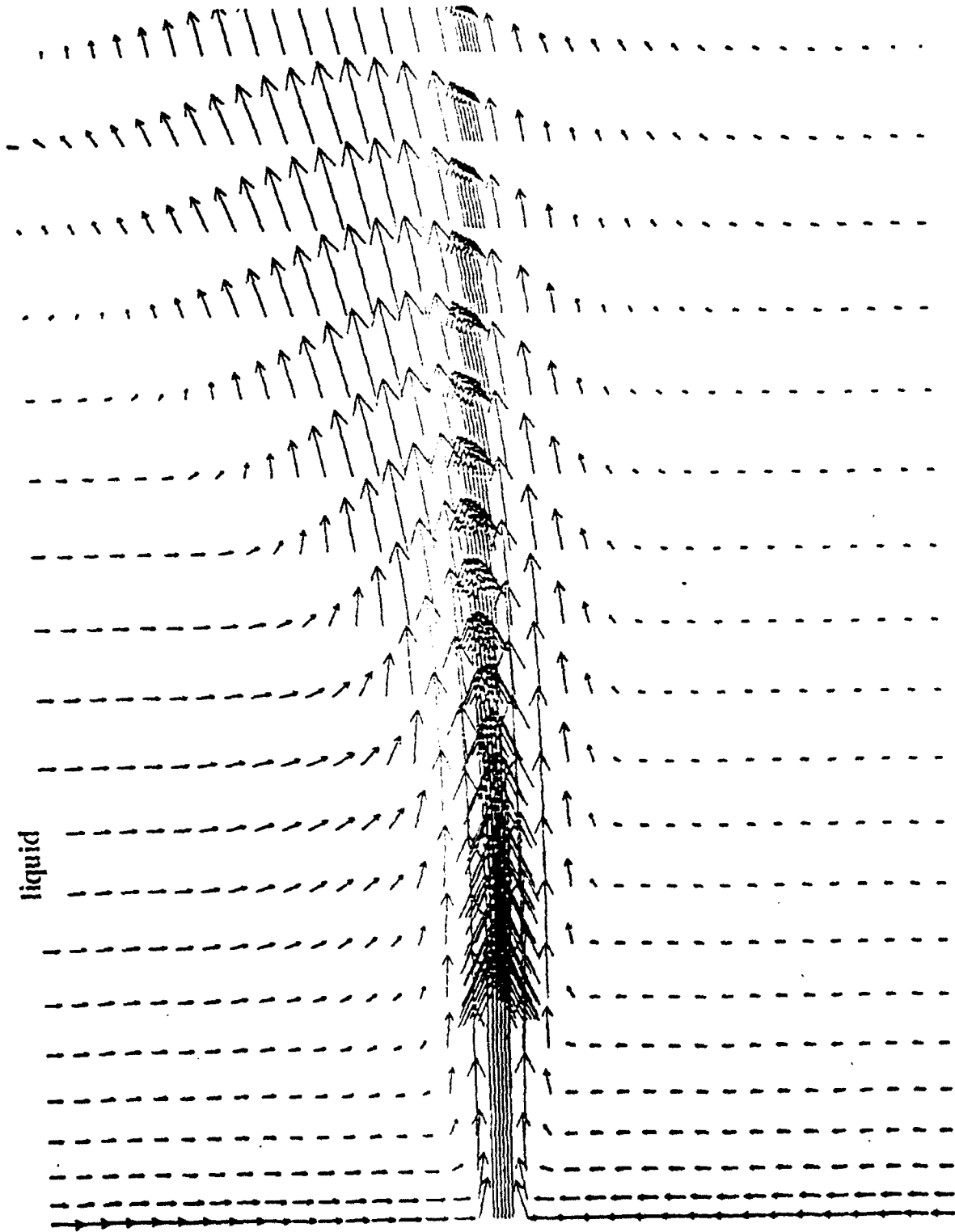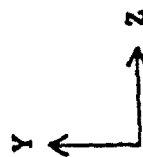
$\longrightarrow$: 2.00 m/s.

K-EP, PLANAR JET, ELLIPTIC, FABIAN, 1 PHASE.

PHOENICS

Figure 11   Vector Plot of the Gas Velocity of the Inclined Jet ($\theta = 45°$)

$\theta = 45$ degrees

gas
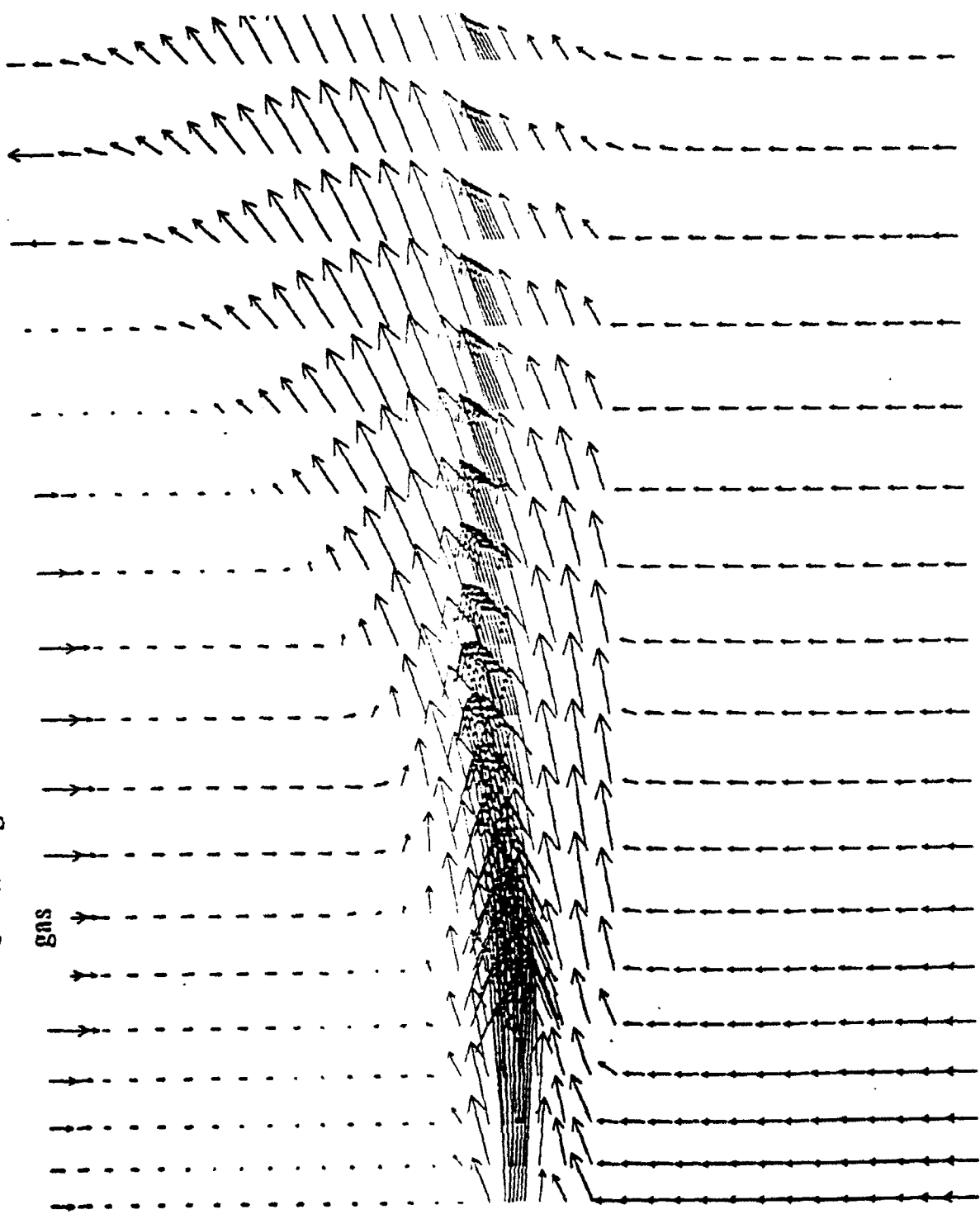
$\bar{u}_g$ (45°)
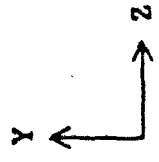
$\longrightarrow$: 2.00 m/s.

K-EP, PLANAR JET, ELLIPTIC, FABIAN, 1 PHASE,

PHOENICS
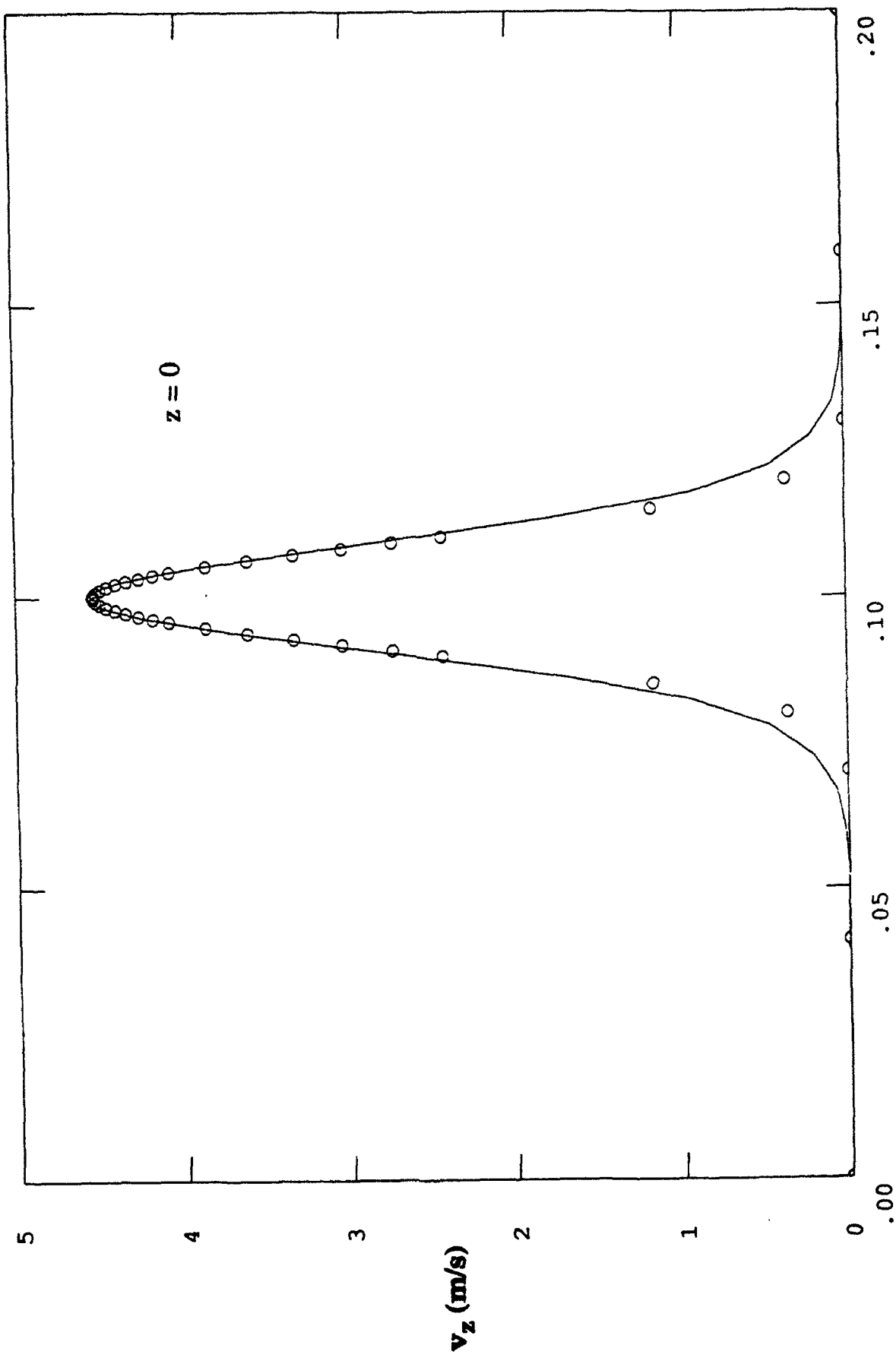
Figure 12 Axial velocity as a function of the lateral coordinate (y = 0.1 m corresponds to the jet center plane) - Inlet conditions.
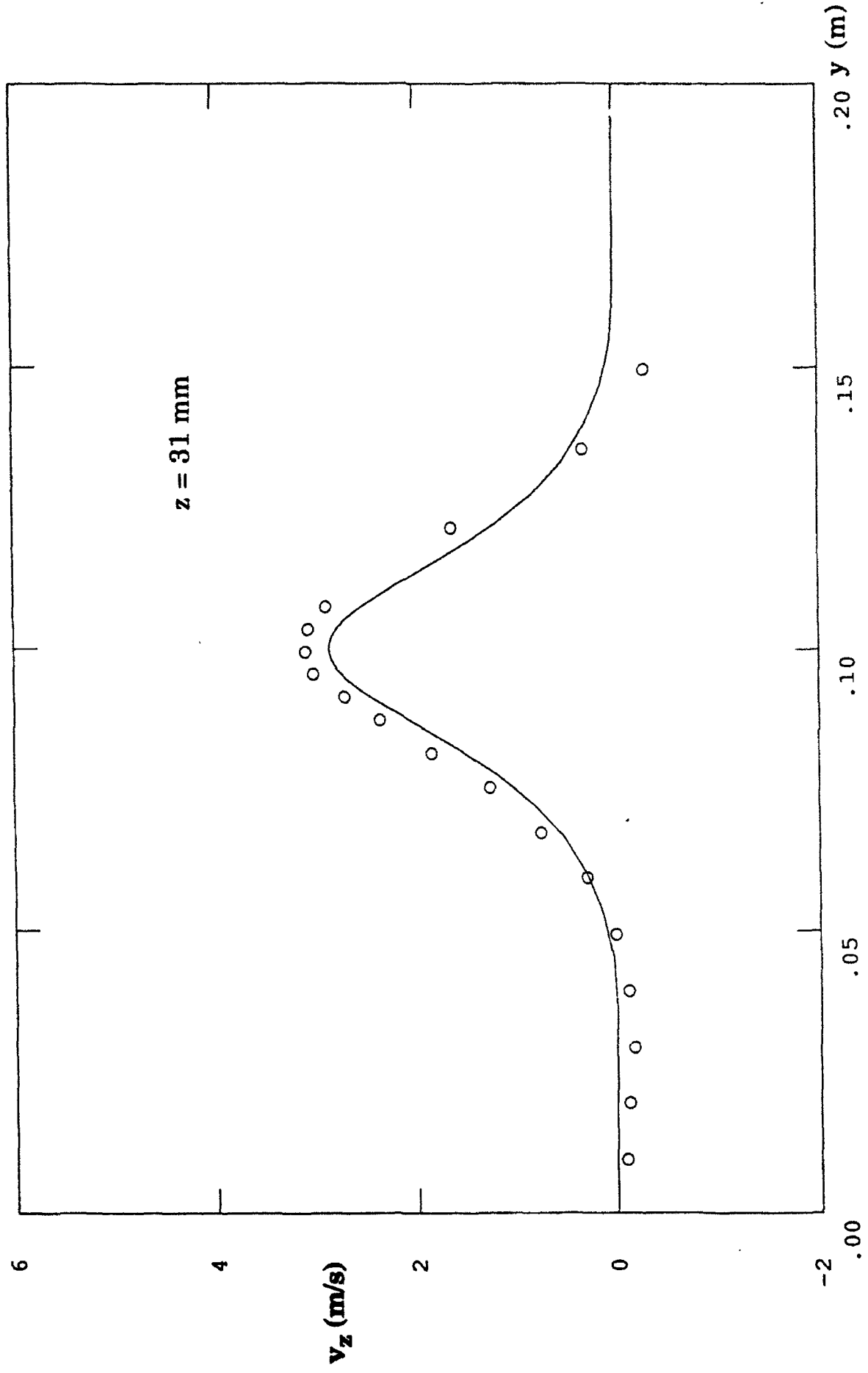
Figure 13 Axial velocity as a function of the lateral coordinate (y = 0.1 m corresponds to the jet center plane. The circles, o, are experimental results)
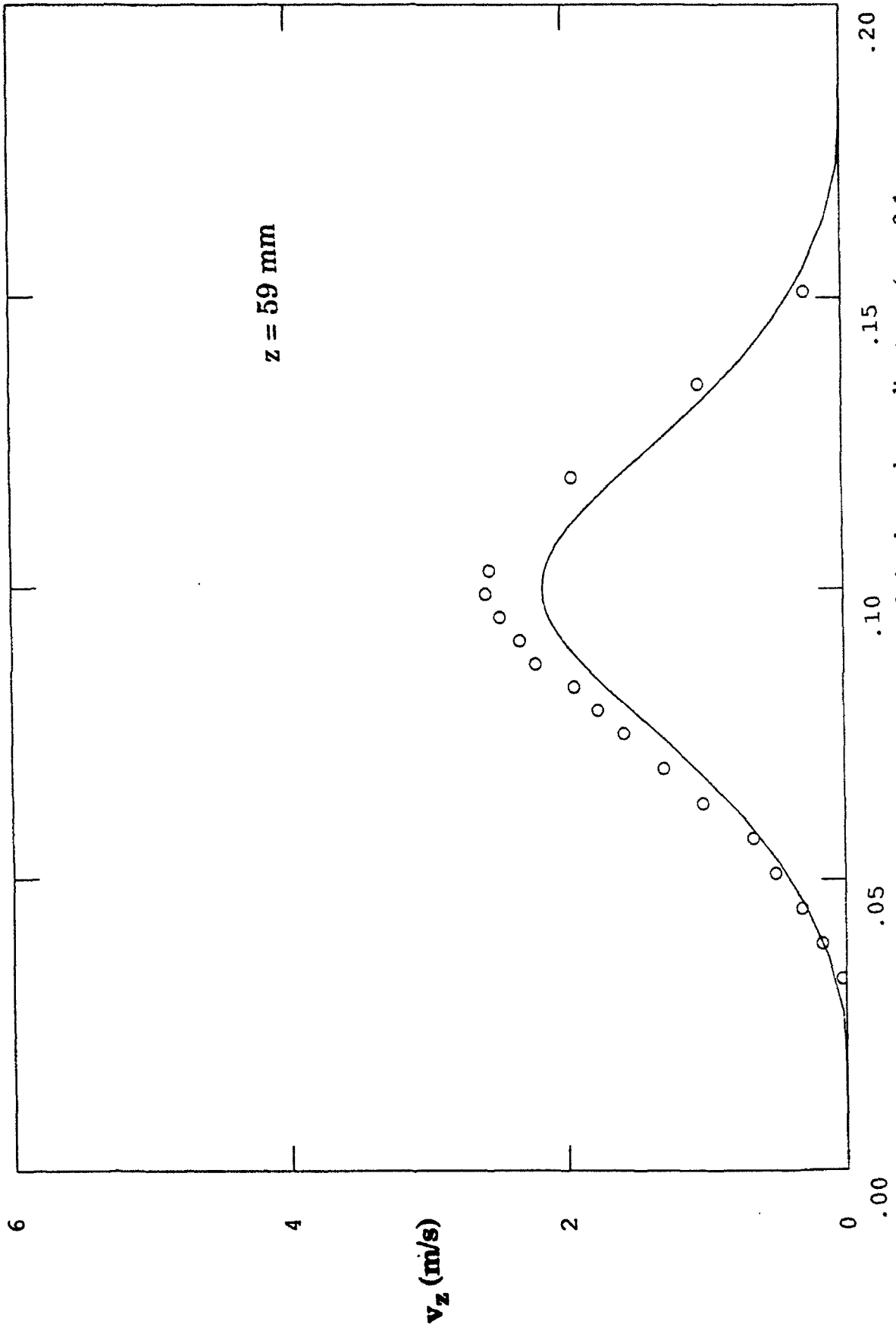
Figure 14 Axial velocity as a function of the lateral coordinate. (y = 0.1 m corresponds to the jet center plane. The circles, O, are experimental results)
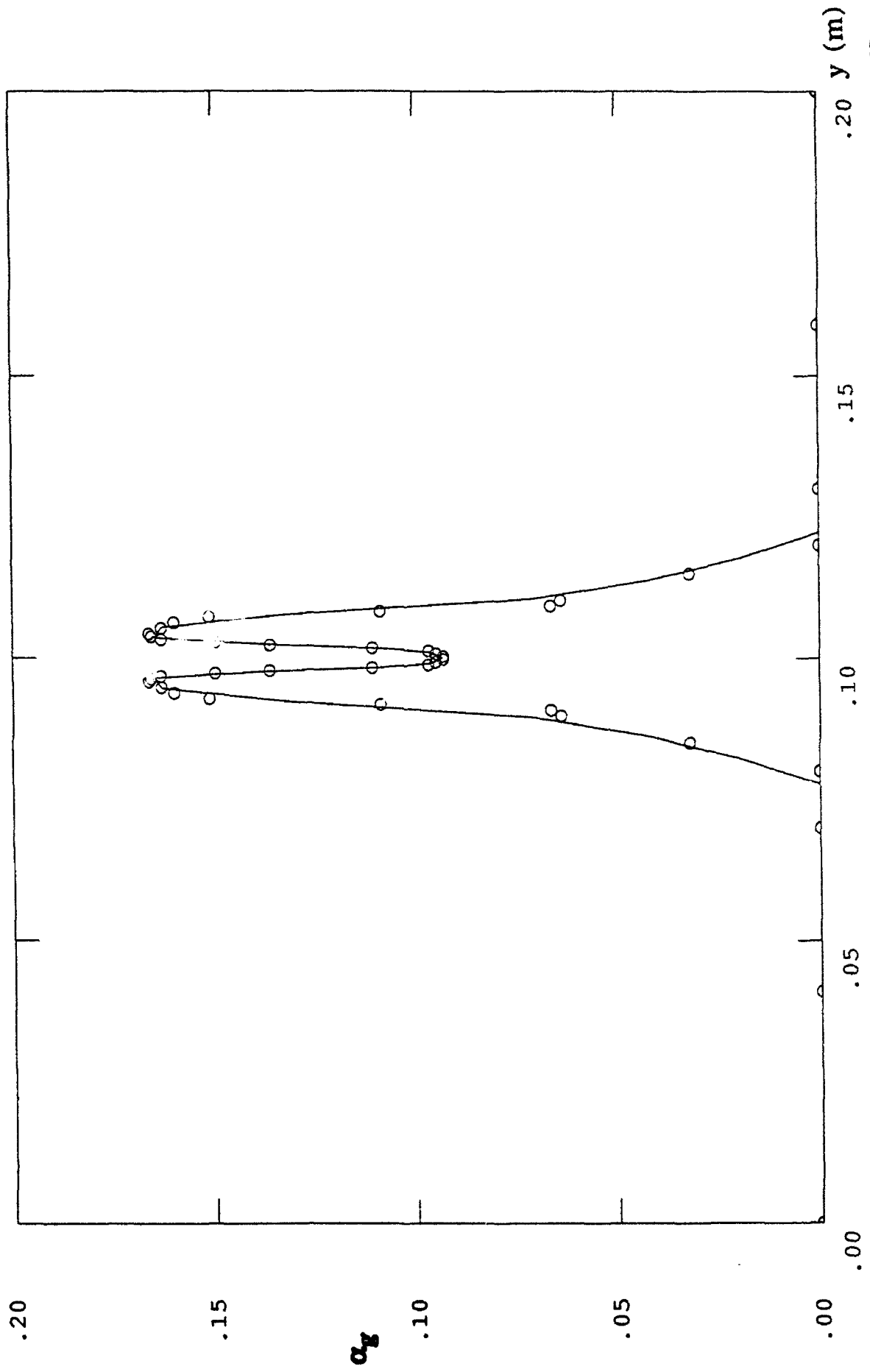
Figure 15 Void fraction as a function of the lateral coordinate. (y = 0.1 m corresponds to the jet center plane) - Inlet conditions
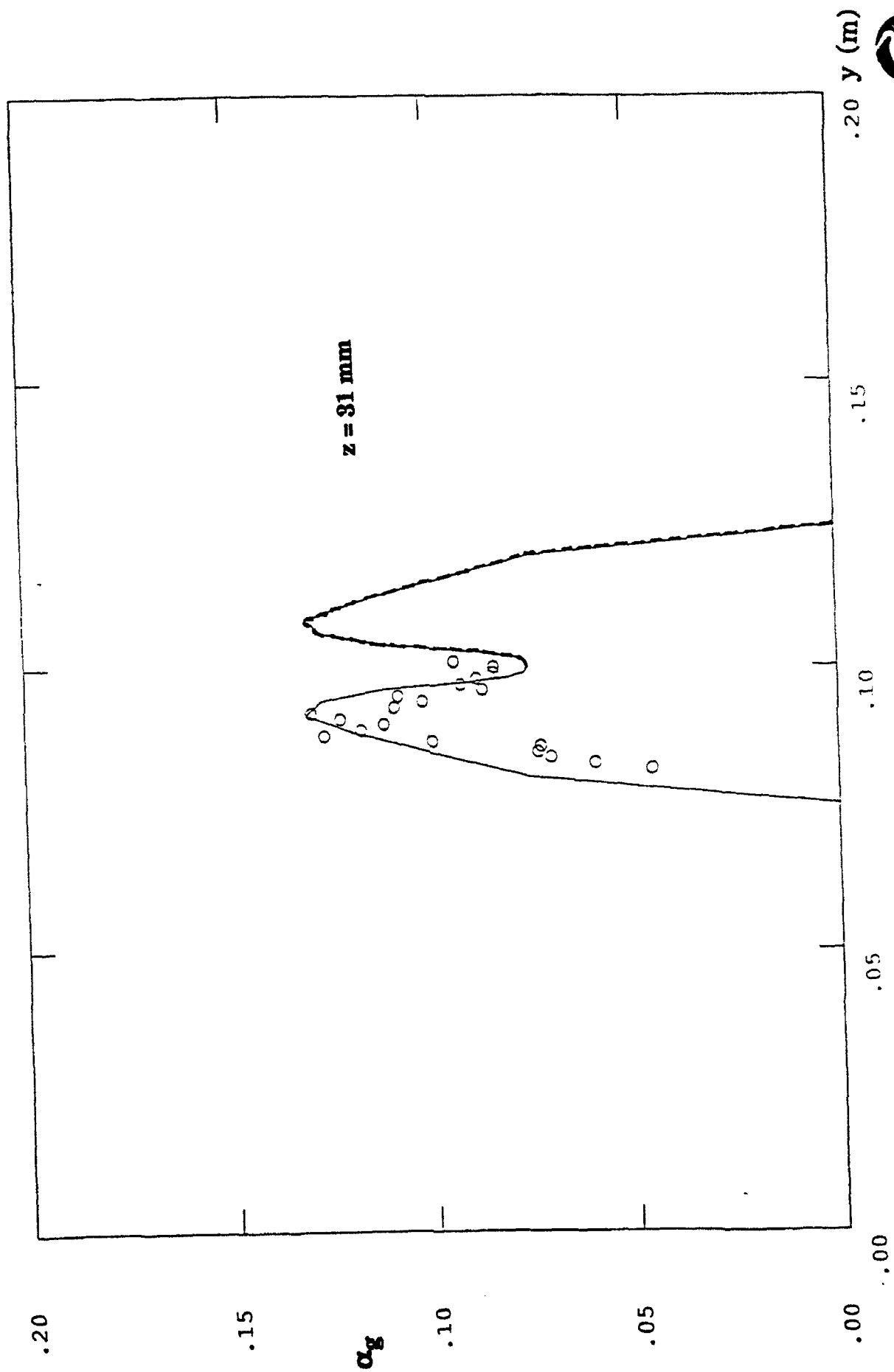
Figure 16 Void fraction as a function of the lateral coordinate. (y = 0.1 m corresponds to the jet center plane. The circles, o, are experimental results)
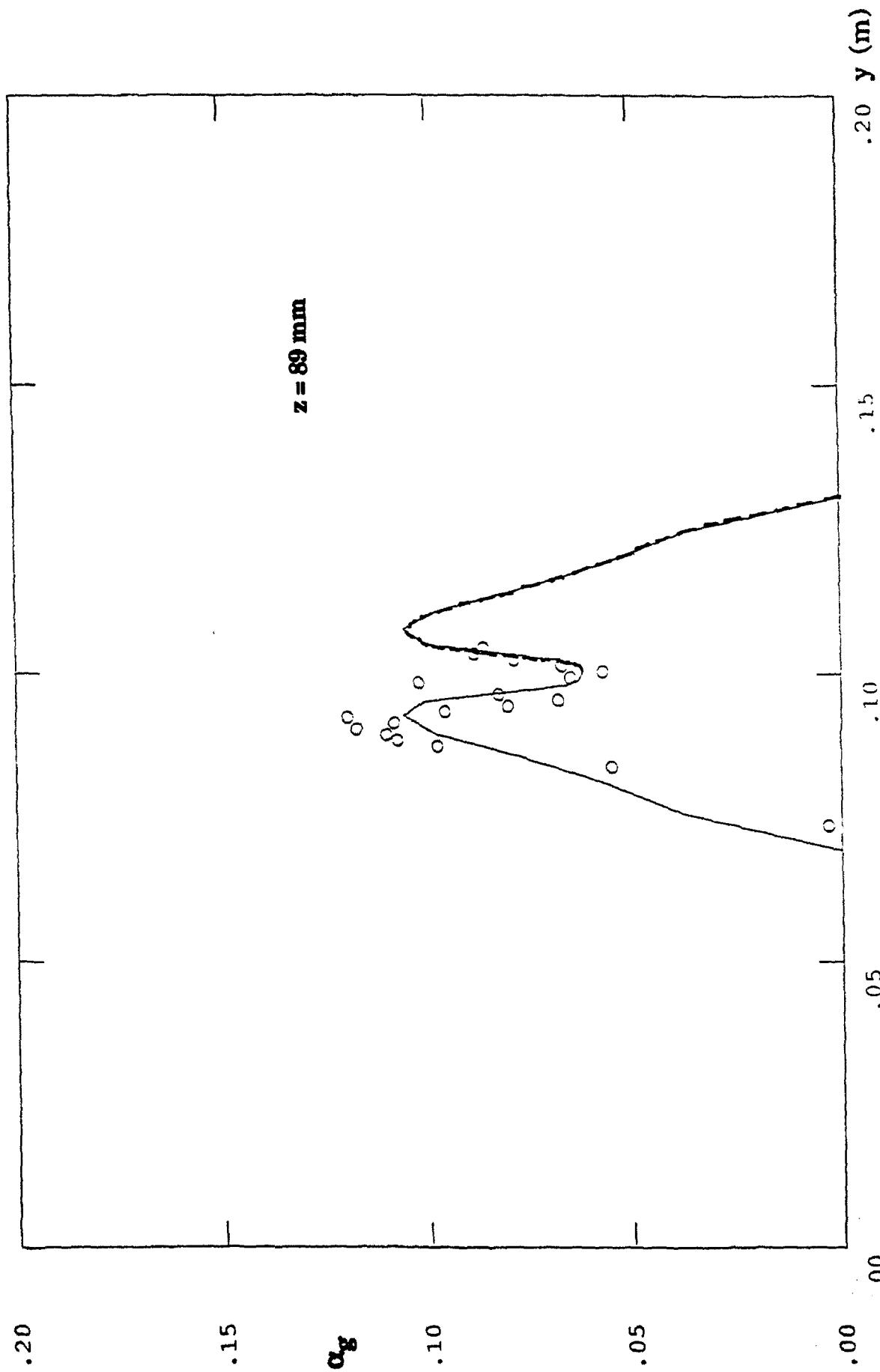
Figure 17 Void fraction as a function of the lateral coordinate. (y = 0.1 m corresponds to the jet center plane. The circles, o, are experimental results)

z = 89 mm